nature communications

Article

https://doi.org/10.1038/s41467-025-66975-3

Early intrinsic excitability plasticity of neocortical engram neurons defines memory formation and precision

Received: 30 January 2025

Accepted: 20 November 2025

Published online: 05 December 2025

Check for updates

Senka Hadzibegovic[1,2,6], Liangying Zhu[1,2,6], Melanie Ginger[1,2], Maria Gueidão Costa[1,2,3], Paula Alvarez Menendez[1,2], Rafaël De Sa[1,2], Katy Le Corf[1,2], Yves Le Feuvre[1,2], Olivier Nicole[2,4], Bruno Bontempi[2,5,7] ✉ & Andreas Frick[1,2,7] ✉

Neocortical memory engrams are thought to mature via strengthened interconnectivity, yet synaptic plasticity alone cannot explain the dynamic vividness of enduring memories. Neuronal intrinsic excitability (IE) plasticity has been touted as an early priming mechanism that renders engram neurons susceptible to ongoing plastic processes and later encoding events. Here, we reveal that learning-induced IE plasticity of nascent anterior cingulate cortex (ACC) engram neurons is a permissive mechanism for the formation and specificity of remote memories. Using *c-fos*-dependent genetic/viral targeting in mice, we found that contextual fear learning triggered a time-limited increase in ACC engram IE during the early phase of memory formation. Remarkably, chemogenetically hyperpolarizing these neurons within—but not outside—the IE plasticity window strengthened consolidated memories, enhanced their context-precision, and prevented interference-induced engram reallocation. Thus, IE plasticity in nascent ACC engram neurons acts as an essential tagging mechanism that determines the fate and dynamic content of remote memories.

Associative memories are gradually embedded within neocortical circuits during systems-level memory consolidation, the process by which remote memories acquire stability and persistence over time[1,2]. Early (during learning) tagging of the same cortical circuits that will later act as the permanent repository of memory engrams has been identified as a prerequisite for successful consolidation[3–6]. Cortical memory engrams are thus thought to undergo a time-dependent maturation process from an initially immature (dormant, non-accessible) to an active (retrievable) state[7,8]. However, the specific processes regulating engram transformation and enduring memory storage remain elusive.

The allocation of neurons to a given memory engram does not occur randomly. Instead, highly excitable neurons within a connected ensemble are preferentially earmarked for integration into an engram[9,10]. In corollary, learning-induced changes in neuronal intrinsic excitability (IE) could provide a key regulatory determinant for engram formation during memory consolidation. Neuron-wide IE plasticity has been described in several brain regions, including the neocortex, following learning paradigms[11–14]. However, while changes in the synaptic strength and connectivity map of engram ensembles are widely viewed mechanisms for storing enduring memories[15,16], the role of IE plasticity in this process is unknown. Neuron-wide IE plasticity would tune the responsiveness of that neuron to the majority of its synaptic inputs (i.e., synaptic penetrance [17]) and might prime it to undergo further plasticity, such as in synaptic strength and connectivity[17]. As a result, this mechanism may dictate the fate of engram neurons during

[1]INSERM U1215, Neurocentre Magendie, Bordeaux, France. [2]University of Bordeaux, Bordeaux, France. [3]University of the Basque Country, Leioa, Spain. [4]CNRS, IINS, UMR 5297, Bordeaux, France. [5]CNRS, INCIA, UMR 5287, Bordeaux, France. [6]These authors contributed equally: Senka Hadzibegovic, Liangying Zhu. [7]These authors jointly supervised this work: Bruno Bontempi, Andreas Frick. ✉e-mail: bruno.bontempi@u-bordeaux.fr; andreas.frick@inserm.fr

systems memory consolidation and permit the establishment of cortical enduring memories. However, neuron-wide IE plasticity would not function as an effective persistent mechanism for storing lasting memories, as it would significantly diminish the storage capacity of these neurons[11,18]. To fulfill this suggested role, we hypothesized that associative learning tasks activate anterior cingulate cortex (ACC) engram ensembles and trigger neuron-wide IE plasticity within these ensembles. These changes occur as a consequence of early activation (i.e. upon encoding) of these cortical neurons, are transient (restricted to the early phase of memory consolidation), and are required as a permissive mechanism to enable the enduring storage of remote memories within the engram network.

Here, we show that contextual fear learning triggers a transient increase in the neuron-wide IE of ACC engram neurons, lasting several days and returning to baseline by the end of the early systems-consolidation phase. Pharmacogenetic hyperpolarization or depolarization of these engram ensembles bidirectionally modulates memory maturation and precision, with the efficacy of this intervention correlating with the time course of IE plasticity. Unexpectedly, early-phase hyperpolarization enhances the maturation and strength of remote fear memories, sharpens their contextual precision, and protects engrams from interference-driven reallocation during this vulnerable window. Together, these findings support the view that learning-induced, transient IE plasticity in ACC engram neurons is a permissive mechanism for the formation of enduring memories.

Results

ACC engram neurons are strongly engaged during learning

The prevailing literature suggests a role for the ACC in late but not early phases of memory formation, making it a central hub within the extended cortical network supporting remote memories[7,19]. To explore whether these ACC engram ensembles are already tagged by the learning experience (nascent engram neurons) and their functional role in later memory expression, we employed a *c-fos*-dependent labeling approach that combines double-transgenic "Tet-Tag" mice with virus-mediated expression of a fluorescent marker (mCherry) during contextual fear conditioning (CFC) (Fig. 1a). CFC represents a single event that induces an ethologically relevant enduring fear memory, enabling rigorous temporal control of neuronal labeling. In the presence of doxycycline (dox), labeling was negligible following CFC (Fig. 1b). Conversely, CFC performed during a defined dox off time window led to the expression of mCherry in engaged ACC neurons (Fig. 1b, Supplementary Fig. 1). CFC produced robust levels of conditioned freezing in CFC mice tested either 1 day or 30 days following training, compared to context (CTX) only mice, indicating the formation of a durable fear memory (Fig. 1c, d; Supplementary Fig. 2a).

Robust CFC-induced fluorescence marker expression was present one day following the learning experience and persisted for at least 30 days, demonstrating rapid and stable labeling of putative ACC engram neurons (Fig. 1e). The number of labeled ACC neurons was significantly greater in the CFC condition compared with those where mice were placed in the conditioning environment without the aversive reinforcement of the foot shocks (CTX) or kept in the home-cage (HC) (Fig. 1e). Early memory retrieval (Day 1) of the CFC group did not significantly reactivate these original putative ACC engram neurons when compared to the CTX and HC groups as indicated by a similar percentage of mCherry$^+$ neurons that were also GFP$^+$ (Fig. 1f; Supplementary Fig. 2b, c). Conversely, during remote memory retrieval (Day 30), a substantial proportion of these neurons of the CFC group was reactivated (mCherry$^+$/GFP$^+$), exceeding the levels observed in the CTX and HC groups (Fig. 1f).

These findings indicate that learning tags nascent ACC engram ensembles that are subsequently reactivated during remote fear-memory expression. Conversely, these ensembles are not reactivated during the early phases of memory retrieval; rather, they remain in a dormant state.

Associative learning triggers neuron-wide IE plasticity in ACC engram neurons

Our data show that putative fear-memory-related ACC engram neurons are tagged already during the learning phase. To examine whether this tagging is accompanied by IE plasticity in these neurons, we evaluated their intrinsic properties during the early phase of memory consolidation, one to three days post-CFC. We performed whole-cell recordings of nascent ACC engram neurons (CFC-YFP$^+$ neurons, Fig. 2a) within acute ACC brain slices (Fig. 2b), focusing on thick-tufted layer 5 (L5) pyramidal tract (PT) neurons (Fig. 2c), which represent a major type of neocortical output neurons. We probed the plasticity of their intrinsic properties by comparing them with labeled neurons from the CTX group (CTX-YFP$^+$ neurons) to identify changes triggered specifically by the learning experience rather than by background activity or unrelated experiences.

We discovered that CFC induced a significant increase in the neuron-wide IE of putative ACC engram neurons compared to control neurons (Fig. 2d–k). This increased excitability was expressed as a greater number of action potentials (APs) triggered by injected current (Fig. 2d). In addition, individual APs were elicited at a lower threshold (Fig. 2e), displayed a higher amplitude (Fig. 2f), were broader (increased half-width; Fig. 2g), and exhibited a reduced upstroke velocity (max dv/dt; Fig. 2h). In agreement with the hyperpolarized shift in the AP threshold, the minimum current to induce an AP (rheobase) was reduced (Fig. 2i). Furthermore, the membrane time constant (tau) was prolonged, widening the temporal window for the integration of synaptic inputs (Fig. 2j). Finally, the amplitude of the medium after-hyperpolarization (mAHP) following a train of APs was reduced for the highest AP frequencies tested (Fig. 2k). However, this reduced mAHP amplitude had no obvious impact on the AP adaptation during a train of APs (Supplementary Fig. 3).

To probe potential compensatory changes in ACC neurons within the same network but outside the fear engram, we assessed IE in neighboring, unlabeled neurons from CFC mice (CFC-YFP$^-$ neurons). This analysis revealed that while some IE measures resemble those of CFC-YFP$^+$ neurons, others resemble CTX-YFP$^+$ neurons, and most parameters fall between these two groups (Supplementary Table 1). This suggests that some unlabeled neurons belong to the engram pool but were not tagged due to incomplete AAV transduction.

Our results show that CFC leads to a plastic increase in the neuron-wide IE of the L5-PT subnetwork of nascent ACC engram neurons. Notably, this IE plasticity is evident one day post-CFC and persists for at least three days.

Neuron-wide IE plasticity is expressed during the early, but not late, phase of memory consolidation

Since neuron-wide IE plasticity is not a suitable permanent storage mechanism, we predicted that this form of plasticity should be transiently expressed during the early, but not late phase, of memory consolidation when memories have matured and are mostly consolidated (> 14 days post-CFC). To test this, we assessed the intrinsic properties of CFC-labeled L5-PT neurons at 15–17 days post-CFC (Fig. 3, Supplementary Table 2).

These measures confirmed our prediction, showing that neuron-wide IE plasticity has returned to control values (i.e., neurons tagged in the CTX group) during the late phase of memory consolidation. Thus, at 15–17 days post-CFC, the IE features were similar between putative engram ensembles (CFC-YFP$^+$), neighboring CFC-YFP$^-$ and control neurons (CTX-YFP$^+$) of the ACC (Supplementary Fig. 4a–l, Supplementary Table 2). Accordingly, the following IE measures of putative engram ensembles (CFC-YFP$^+$) differed significantly between the early and late phases of memory consolidation (values were normalized to

https://doi.org/10.1038/s41467-025-66975-3

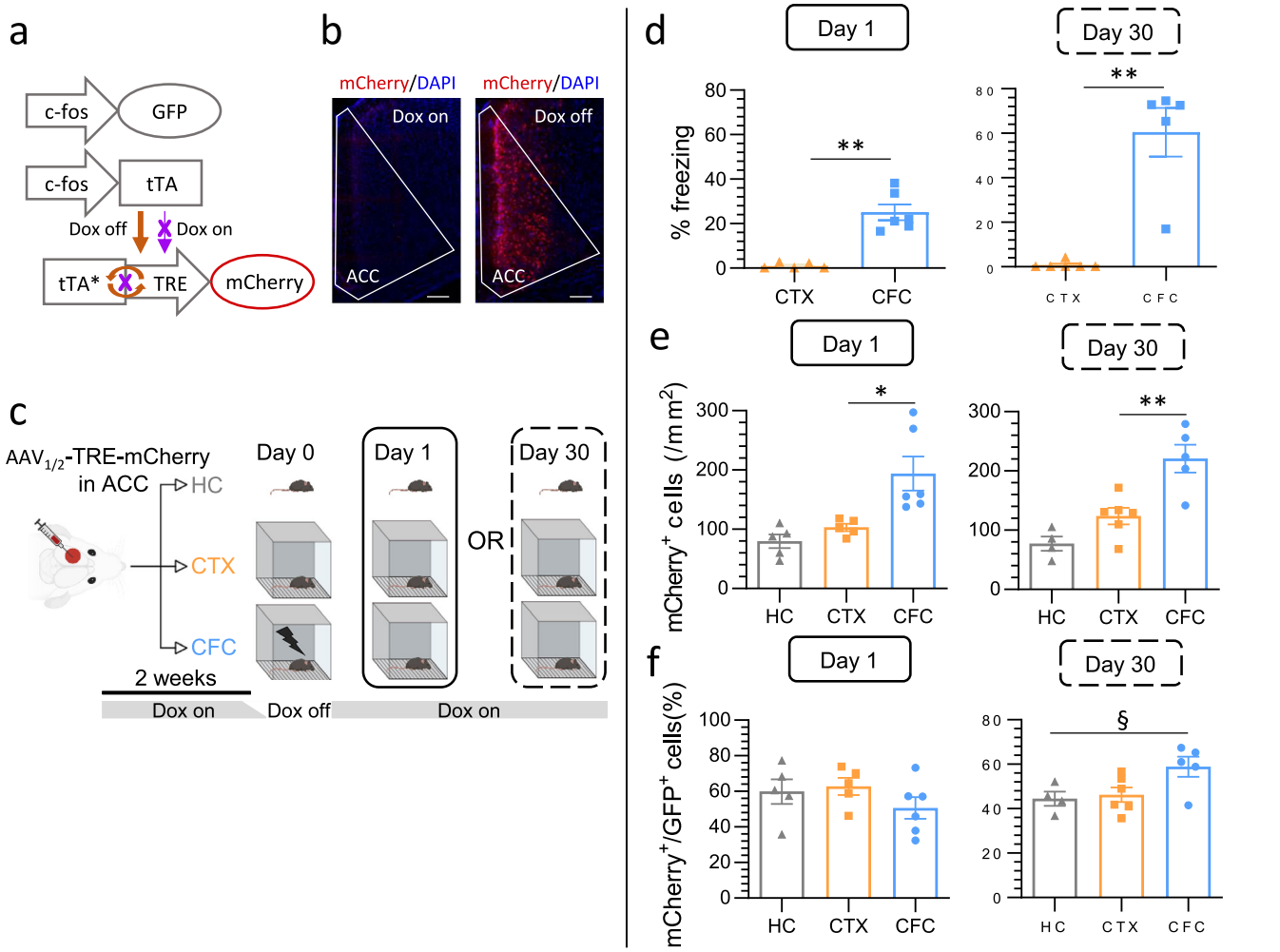

Fig. 1 | ACC engram ensembles are tagged by learning and reactivated during remote memory expression. a Long-lasting tagging of ACC engram neurons using the Tet-Tag mouse coupled with $AAV_{1/2}$-TRE-iDREADD-mCherry (TRE-mCherry) infusions. Doxycycline removal enables tTA (tetracycline transactivator)-driven persistent mCherry expression under the *c-fos* promoter, with a transient expression of GFP. **b** Representative images showing mCherry-tagging in the absence of doxycycline (Dox off). Scale bar: 150 μm. **c** CFC (contextual fear conditioning) and CTX (context only) groups were trained during the dox-off period and tested for retrieval 1 (recent memory) or 30 days (remote memory) later (**d**–**f**, Day 1: CTX, $n = 5$ mice, CFC, $n = 6$ mice; Day 30: CTX, $n = 6$ mice, CFC, $n = 5$ mice). Home-cage (HC) served as additional control (**e,f** Day 1: $n = 5$ mice; Day 30: $n = 4$ mice). **d** CFC produced robust levels of freezing in mice tested 1 ($U = 0$, $p = 0.004$, Cohen's $d = 3.67$) or 30 days ($U = 0$, $p = 0.004$, Cohen's $d = 3.64$) following training. **e**, ACC neurons were strongly engaged during CFC (one day after training; K-W = 11.58, $p = 0.0001$; Dunn's multiple comparison test: HC vs CTX, $p = 0.319$, HC vs CFC, $p = 0.001$, CTX vs CFC, $p = 0.024$, Cohen's d = 2.09) and this tag was stably expressed for at least 30 days ($F(2, 12) = 15.93$, $p = 0.0004$; Tukey's multiple comparisons test: HC vs CTX, $p = 0.203$, CI[−114.6, 21.46], HC vs CFC, $p = 0.0004$, CI[−214.2, −72.79], CTX vs CFC, $p = 0.004$, CI[−160.7, −33.11], Cohen's d = 1.25). **f** ACC reactivation assessed by the percentage of $mCherry^+$ co-expressing GFP^+. CFC neurons showed greater reactivation upon remote ($F(2, 13) = 4.13$, $p = 0.043$; Tukey's multiple comparisons test: HC vs CTX, $p = 0.942$, CI[−16.44, 12.83], HC vs CFC, $p = 0.065$, CI[−29.58, 0.8383], CTX vs CFC, $p = 0.074$, CI[−26.29, 1.163], Cohen's d = 0.88), but not recent ($F(2, 13) = 1.15$, $p = 0.347$; Tukey's multiple comparisons test: HC vs CTX, $p = 0.942$, CI[−26.29, 20.48] HC vs CFC, $p = 0.536$, CI[−13.14, 31.63], CTX vs CFC, $p = 0.353$, CI[−10.24, 34.54], Cohen's d = 0.26) memory retrieval compared to CTX and HC. Means ± SEMs are shown with individual mouse values. Significance was calculated using two-sided Mann-Whitney test (d) or one-way ANOVA or Kruskal-Wallis test (e, f), and indicated in the figures as follows: *p < 0.05, **p < 0.01, and §p < 0.05 for interaction effect. See also Supplementary Fig. 2. Created in BioRender. Zhu, L. (2025) https://BioRender.com/jtnacj6 and https://BioRender.com/0uwbq6b.

those of CTX during early and late phases, respectively; Fig. 3b–g and Supplementary Fig. 5a–f): AP number triggered by current injection (greater during the early consolidation phase; Fig. 3b), AP peak amplitude (increased; Fig. 3c), AP half-width (increased; Fig. 3d), rheobase (reduced; Fig. 3e), tau (increased; Fig. 3f), mAHP amplitude (reduced; Fig. 3g), and AP adaptation (reduced; Supplementary Fig. 5b). Conversely, there was no significant difference in the RMP (Supplementary Fig. 5c), input resistance (Supplementary Fig. 5d), AP upstroke velocity (max dV/dt; Supplementary Fig. 5e), and only a trend for the AP threshold (more hyperpolarized during the early phase; Supplementary Fig. 5f).

To refine the decay timeline, we probed these physiological parameters at an intermediate 8-9-day time point. By 8–9 days, most electrophysiological parameters were indistinguishable from baseline (Supplementary Fig. 6) and the late phase (Supplementary Fig. 7).

Collectively, these data show that the learning-induced neuron-wide IE plasticity of putative ACC engram neurons is expressed during the early, but not late, phase of memory consolidation, and has largely returned to baseline by 8-9 days after CFC.

The IE state of ACC nascent engram neurons is crucial for the formation of remote fear memory

According to our hypothesis, neuron-wide IE plasticity is expected to enhance the reactivation of the engram ensemble and permit more enduring plastic changes that require repeated neuronal activation and more time to develop. Consequently,

https://doi.org/10.1038/s41467-025-66975-3

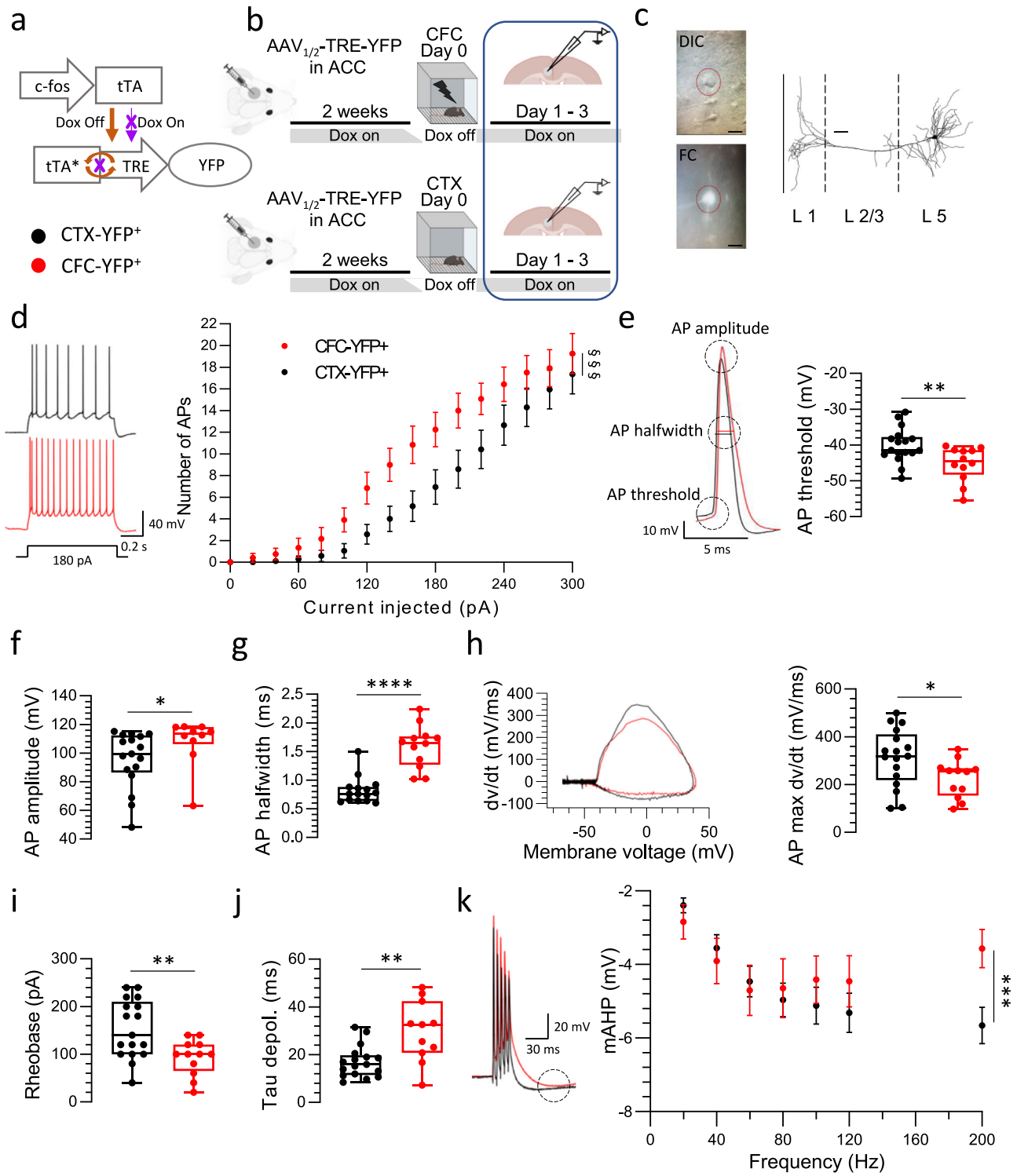

modulating the excitation state of ACC engram ensembles during the CFC-induced IE plasticity phase should interfere with this functional role and impact the formation of enduring fear memories. We probed this by using a pharmacogenetic approach. Employing our tet-tagging systems, we expressed either inhibitory (i) or excitatory (e) designer receptors exclusively activated by designer drugs (DREADD) selectively in nascent ACC engram neurons following CFC (Fig. 4a). Mice were then treated twice a day for seven consecutive days following CFC with the DREADD ligand, CNO, or vehicle (saline), and finally tested for remote fear memory expression (30 days post-CFC; Fig. 4a). Surprisingly, we found that activation of iDREADD within ACC engram ensembles (including the L5-PT subnetwork) during the early consolidation phase enhanced remote fear memory expression (manifested as increased freezing) in these mice (iDREADD-CNO group) when compared to control (i/eDREADD-saline group; Fig. 4b).

These data suggest that pharmacogenetic hyperpolarization of ACC engram neurons during the early phase of memory consolidation, when they display increased neuron-wide IE plasticity, can enhance enduring fear memory formation.

Fig. 2 | Contextual fear conditioning triggers IE plasticity in ACC nascent engram ensembles. a Tagging strategy for ACC engram neurons (visualized by YFP expression). **b** Experimental design. Whole-cell patch-clamp recordings were obtained from YFP$^+$ neurons in CFC and CTX groups 1-3 days after training. **c** (left), Representative images from differential interference contrast (DIC) and fluorescence confocal (FC) microscopy during recording (scale bar 20 µm). (right) Three-dimensional reconstruction of layer 5 (L5) YFP$^+$ neuron. Scale bar: 50 mm. **d**–**k**, Analysis of YFP$^+$ neurons from the CFC ($n = 12$ cells) and CTX groups ($n = 17$ cells). **d** (left) Representative traces of action potentials (APs) induced by a 180 pA current injection. (right) Increase in the number of APs as a function of injected current in CFC compared to CTX (Current x Condition interaction, F(15, 405) = 2.64, $p = 0.0008$, CI[−0.1672, 6.126], Cohen's $d = 0.36$). **e** (left), Example traces of single APs. (right) Decrease in AP threshold in CFC neurons (t(27) = 2.85, $p = 0.008$, CI[1.456, 8.900] Cohen's d = 0.90). **f,g** Increase in AP amplitude (U = 41, $p = 0.027$, Cohen's d = 0.68) and AP half-width (U = 6, p < 0.0001, Cohen's d = 2.48). **h** (left), Example traces for AP upstroke velocity (max dv/dt). (right) Max dv/dt is decreased in CFC neurons (t(27) = 2.21, $p = 0.036$, CI[6.332, 169.0], Cohen's d = 0.86). **i** Reduction in rheobase in CFC neurons (t(27) = 2.99, $p = 0.006$, CI[18.72, 100.5], Cohen's d = 1.17). **j** Increase in Tau in CFC neurons (t(25) = 2.80, $p = 0.098$, CI[−20.32, −5.379], Cohen's d = 1.27). **k** (left), Example traces of medium after-hyperpolarization (mAHP) from a 5-AP-train at 200 Hz. (right) Reduction in mAHP amplitude for high frequencies (Hz x Condition interaction, F(6, 159) = 7.30, p < 0.0001, CI[−1.163, 1.795], Cohen's d = 0.22) in CFC neurons. Box plots show individual values with median (center), lower and upper quartiles (the bounds of the box), and minima and maxima (whiskers) (**e**–**j**) or mean values ± SEM (**d**,**k**). Statistical significance was calculated using repeated measures of two-way ANOVA (d) or Mixed-effects model when there were missing values both followed by Šídák's multiple comparisons test (k) or two-sided unpaired t-test (e-j), $^*p < 0.05$, $^{**}p < 0.01$, $^{***}p < 0.001$, $^{****}p < 0.0001$, and $^{§§§}p < 0.001$ for interaction effect. See also Supplementary Fig. 3. Created in BioRender. Zhu, L. (2025) https://BioRender.com/jtnacj6, https://BioRender.com/9vr15p6 and https://BioRender.com/xpj3wfh.

Context specificity of remote fear memory is malleable during the early IE plasticity phase

In addition to strengthening remote fear memory, we wondered whether modulating the excitation state of ACC engram ensembles during the early phase of memory consolidation could also improve the precision of the remote fear memory for the specific context. We assessed precision by comparing memory specificity for the original context (Context A) versus a new context (Context B) (Fig. 4a). Instead of repeated testing, mice were divided into separate groups for remote retrieval in either Context A or Context B because we found that successive retrieval in both contexts attenuated fear expression in the second context (Supplementary Fig. 8a–c). These experiments showed that the iDREADD/CNO group discriminated better between the two contexts compared to the control group, displaying an improved Context A-specific fear memory (Fig. 4b, c). The improvement in memory precision resulted from an increase in freezing behavior in Context A, coupled with a decrease in freezing behavior in Context B (Fig. 4c). In contrast, activating eDREADD in tagged ACC engram neurons eliminated the capacity to discriminate between the original and the new context (Fig. 4b, c). The differences in memory precision and strength between the three groups could neither be explained by the original freezing score during CFC (Supplementary Fig. 9a and b), nor by the number of engram neurons that expressed DREADD (Supplementary Fig. 9c).

We then asked whether the increased memory strength/precision induced by iDREADD-mediated hyperpolarization of ACC engram neurons (Fig. 4b, c) would be reflected in a greater reactivation of these neurons during remote memory retrieval. Indeed, the reactivation ratio (% colocalization mCherry$^+$/GFP$^+$ neurons) was significantly greater compared to the saline or eDREADD condition (Fig. 4d). In contrast, the number of retrieval-activated neurons itself was not altered by chemogenetic manipulation (Supplementary Fig. 9d).

Our results suggest that the IE plasticity of nascent ACC engram ensembles during early memory consolidation is crucial for the permanent storage and precision of fear memories. Any modulation of the excitation state of ACC engram ensembles during the IE plasticity phase crucially influences these memory features in a bidirectional manner; chemogenetic hyperpolarization effectively improves memory strength and specificity and results in an enhanced maturation of the nascent ACC engram ensemble, whereas chemogenetic depolarization has the opposite effect.

Modulating the IE state of matured ACC engram neurons does not affect memory expression

We next examined whether the effectiveness of manipulating the excitation of ACC engram neurons to improve memory formation was dependent on the phase of memory consolidation. To this end, we delayed the DREADD-induced excitation modulation of ACC engram neurons by administering CNO 15 to 22 days following CFC. This timing allowed us to selectively target the late phase of memory consolidation when the IE plasticity had returned to control levels (Fig. 3). Consistent with the previously observed temporal course of IE plasticity, we observed no functional consequence for memory performance or context precision upon remote memory retrieval by either iDREADD or eDREADD activation during this late time window (Fig. 4f, g and Supplementary Fig. 10a–d). Likewise, ACC engram ensemble reactivation was not affected by excitability modulation at this late phase of memory consolidation (Fig. 4h).

Our data show that the time course of the IE plasticity of ACC engram ensembles coincides with the temporal window of effective neuronal modulation of fear memory formation and precision, revealing that the late phase of the consolidation process has become resistant to such manipulation.

The impact of interference on memory performance depends on the consolidation phase

Interference occurring shortly after training, during the early phase of memory consolidation, has been shown to impair remote memory formation, likely by reallocating more excitable engram neurons into a new ensemble[9]. Concurring with this, we found that retroactive interference in the form of exposure to an enriched environment 1 day following CFC (Early–INT; Fig. 5a) impaired memory formation by decreasing freezing during remote memory retrieval compared to the control condition (day 30; Fig. 5b). In contrast, the same interference experience administered during the late phase of memory formation (15 days post-CFC; Late–INT) had no impact on remote memory performance (Fig. 5a, b). Freezing levels during CFC were similar between the different groups, ruling out differences in memory acquisition as a potential confounding factor (Supplementary Fig. 11a, b).

These data demonstrate that, similarly to the DREADD manipulation, the impact of an ethologically relevant experiential factor, such as interference, on memory formation phase-locks to the transient time course of neuron-wide IE plasticity of ACC engram ensembles.

Precocious manipulation of IE plasticity protects memory formation from interference

We next asked whether chemogenetic hyperpolarization of ACC engram neurons during the early phase of memory consolidation could prevent remote memory impairment caused by an early interference experience. To address this, we administered CNO for the first seven days following CFC to activate iDREADD on ACC engram neurons, exposed the mice to interference on day one, and evaluated remote (30 days post-CFC) memory performance (Fig. 5c). Importantly, this manipulation prevented the interference-induced memory impairment, rescuing the fear

https://doi.org/10.1038/s41467-025-66975-3

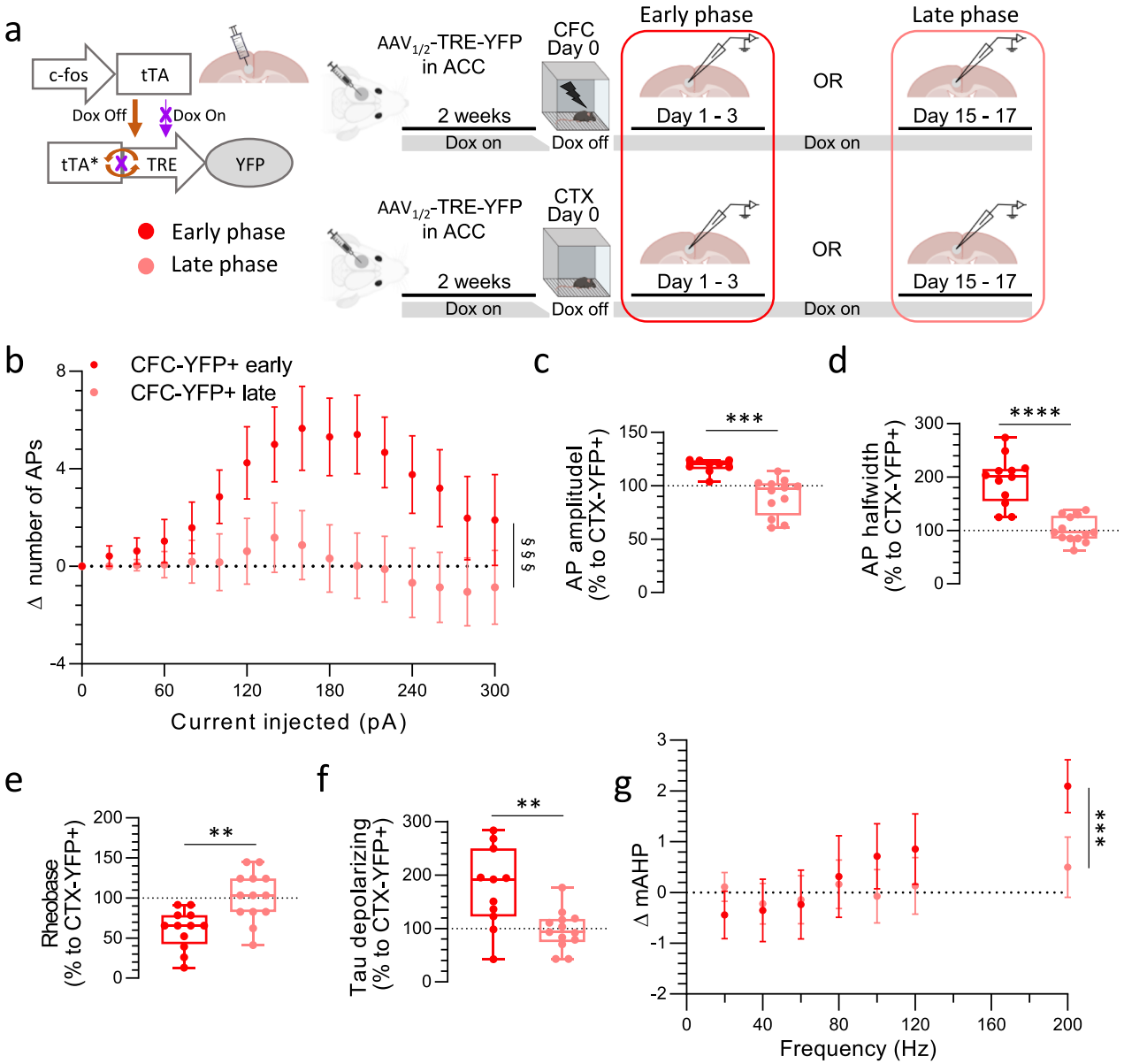

Fig. 3 | Learning-induced IE plasticity of ACC engram neurons is transient. **a** (left) Strategy for tagging of ACC engram neurons visualized by YFP neuronal expression. (right) Experimental design. Whole-cell patch-clamp recordings were performed from tagged (YFP$^+$) L5 pyramidal neurons either during the early phase (1-3 days post-CFC) or late phase (15-17 days post-CFC) of memory consolidation. Data are normalized to values from control (CTX-YFP$^+$) cells for the respective consolidation phases. **b**–**g** Detailed analysis of YFP$^+$ neurons from the CFC groups for each consolidation phase (early phase, $n = 12$ cells; late phase, $n = 13$ cells). Significant differences were found for the number of APs (presented as Δ: difference in the values between CFC-YFP$^+$ and CTX-YFP$^+$; Current x Condition interaction, $F(15, 345) = 2.98$, $p = 0.0002$, CI[-0.08541, 6.050], Cohen's d = 0.38). **b** AP amplitude ($t(19) = 4.62$, $p = 0.0002$, CI[-41.15, -15.48], Cohen's d = 2.16). **c** AP halfwidth ($t(23) = 6.50$, $p < 0.0001$, CI[-122.4, -63.30], Cohen's d = 2.57). **d** rheobase ($t(23) = 3.632$, $p = 0.0014$, CI[17.58, 64.09], Cohen's d = 1.24). **e** Tau depolarizing ($t(23) = 3.39$, $p = 0.003$, CI[-126.9, -30.54], Cohen's d = 1.35). **f** and mAHP amplitude, presented as Δ: difference in the values between CFC-YFP$^+$ and CTX-YFP$^+$ (Hz x Condition interaction, $F(6, 131) = 4.41$, $p = 0.0004$, CI[-1.297, 1.870], Cohen's d = 0.19). **g** Box plots show individual values with median (center), lower and upper quartiles (the bounds of the box), and minima and maxima (whiskers) (**c**–**f**) or mean values ± SEM (**b**,**g**). Statistical significance was calculated using repeated measures of two-way ANOVA (**b**) or Mixed-effects model when there were missing values both followed by Šídák's multiple comparisons tests (**g**) or the two-sided unpaired t-test (**c**–**f**), $^*p < 0.05$, $^{**}p < 0.01$, $^{***}p < 0.001$, $^{****}p < 0.0001$, and § § § $p < 0.001$ for interaction effect. See also Supplementary Fig. 5 and Supplementary Table 3 for statistical analysis of multiple comparisons between early and late phase measurements. Created in BioRender. Zhu, L. (2025) https://BioRender.com/jtnacj6, https://BioRender.com/9vr15p6 and https://BioRender.com/xpj3wfh.

expression levels upon retrieval (Fig. 5d). Freezing levels during CFC were similar between the different groups indicating that there were no differences in memory acquisition that might impact these results (Supplementary Fig. 11c, d). The size of the putative engram that supported the acquisition (Supplementary Fig. 11e) and retrieval of the associative memory was also similar between groups (Fig. 5e and Supplementary Fig. 11f).

To address whether iDREADD-mediated hyperpolarization of ACC engram neurons prevents their reallocation to a new engram during early consolidation, we quantified mCherry-c-Fos co-expression after the INT protocol. Compared to the INT-saline group, CNO caused a reduction in co-labeling (Fig. 5f, g), while the numbers of iDREADD-positive (mCherry$^+$) or c-Fos-positive cells during INT were unchanged (Supplementary Fig. 11g-i).

https://doi.org/10.1038/s41467-025-66975-3

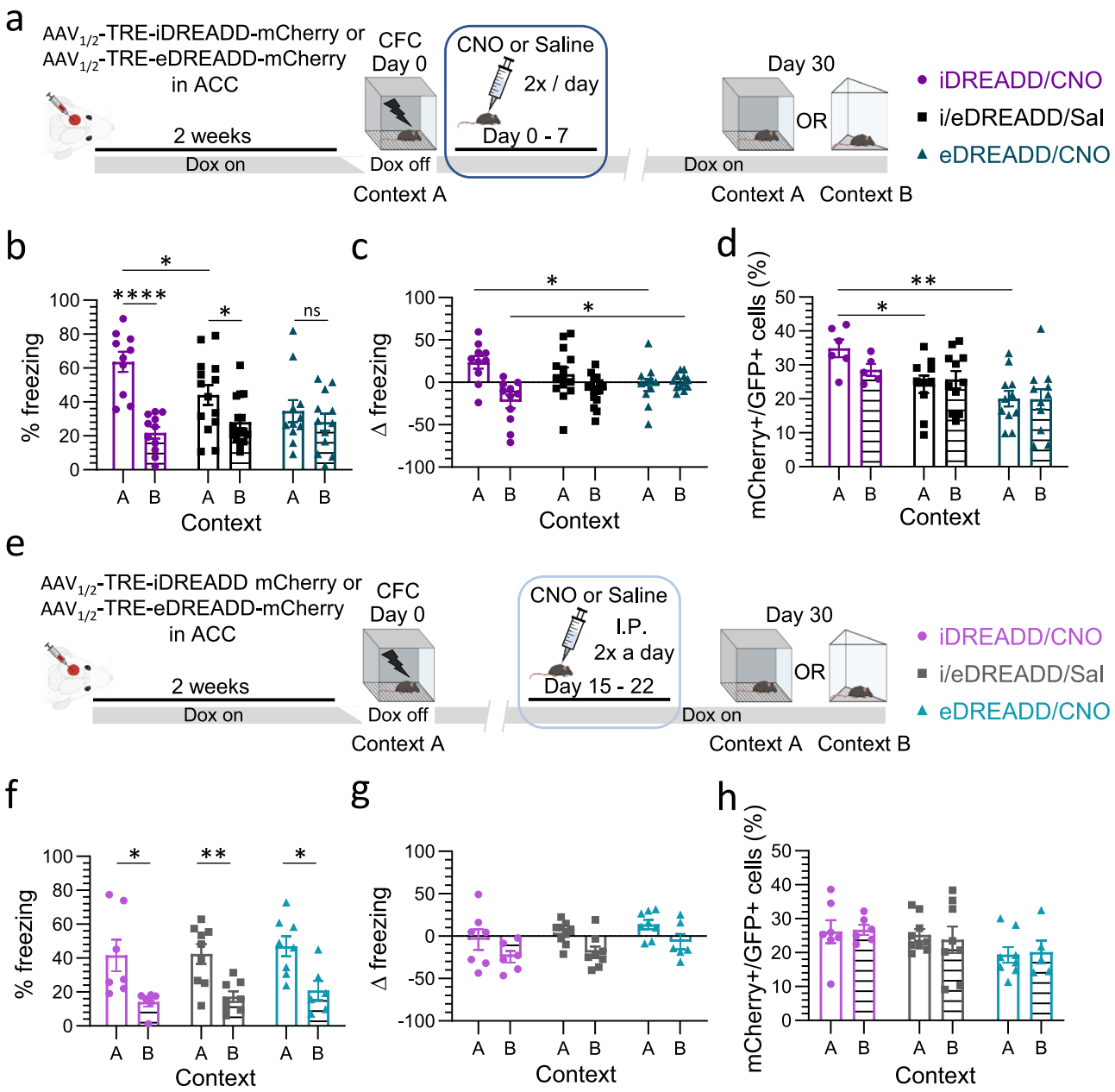

Fig. 4 | Modulating IE of nascent ACC engram neurons determines the formation and precision of remote fear memories. a Experimental design. Assessing the consequence of manipulating the IE of ACC engram ensembles during the early phase of memory consolidation on context precision of remote fear memories (day 30 post-CFC). **b** Results for the three groups (iDREADD/CNO (A: $n = 10$ mice, B: $n = 11$ mice), eDREADD/CNO (A: $n = 11$ mice, B: $n = 12$ mice), and i/eDREADD/Sal (A: $n = 14$ mice, B: $n = 16$ mice)) are expressed as the % of time spent freezing during remote memory retrieval (Treatment x Condition interaction, $F(2, 68) = 5.82$, $p = 0.0047$, CI[13.12, 29.79], η^2=0.11). **c** Results from the same mice are presented as Δ freezing (difference in the % of freezing between retrieval and after the last shock during memory acquisition; Treatment x Condition interaction, $F(2, 68) = 6.75$, $p = 0.0021$, CI[9.776, 31.00], η^2=0.14). **d** % of reactivated tagged ACC engram neurons following remote memory retrieval (mCherry$^+$/GFP$^+$ cells; Treatment, $F(2, 48) = 7.82$, $p = 0.0011$, CI[-2.949, 6.377], η^2=0.25, iDREADD/CNO, A: $n = 6$ mice, B: $n = 5$ mice, eDREADD/CNO, A: $n = 11$ mice, B: $n = 11$ mice, and i/eDREADD/Sal, A: $n = 10$ mice, B: $n = 11$ mice). **e** Experimental design. Same as in (**a**) with IE manipulation delivered during the late phase of memory consolidation. **f**, **g** Targeting the late phase of memory consolidation did not alter remote fear memory precision (all groups were able to discriminate context A from context B, iDREADD/CNO, A: $n = 7$ mice, B: $n = 6$ mice, eDREADD/CNO, A: $n = 8$ mice, B: $n = 6$ mice, and i/eDREADD/Sal, A: $n = 9$ mice, B: $n = 8$ mice) as measured by % freezing (Treatment x Condition interaction, $F(2, 38) = 0.02$, $p = 0.9808$, CI[16.28, 36.13], η^2=0.0006) (**f**) and no changes were observed for Δ freezing (Treatment x Condition interaction, $F(2, 38) = 0.02$, $p = 0.9797$, CI[8.498, 33.68], η^2=0.0007) (**g**) in either iDREADD/CNO or eDREADD/CNO mice compared to the i/eDREADD/Sal group. **h** % of reactivated tagged ACC engram neurons during remote memory retrieval (Treatment x Condition interaction, $F(2, 37) = 0.095$, $p = 0.9096$, CI[-4.740, 4.824], η^2=0.004; iDREADD/CNO, A: $n = 7$ mice, B: $n = 6$ mice, eDREADD/CNO, A: $n = 8$ mice, B: $n = 5$ mice, and i/eDREADD/Sal, A: $n = 9$ mice, B: $n = 8$ mice). Means ± SEMs are shown with individual mouse values. Statistical significance was calculated using two-way ANOVA followed by Tukey/Šídák's multiple comparisons test (b-d, f-h), $^*p < 0.05$, $^{**}p < 0.01$, $^{****}p < 0.0001$. See also Supplementary Fig. 9 and 10. Created in BioRender. Zhu, L. (2025) https://BioRender.com/jtnacj6 and https://BioRender.com/0uwbq6b.

https://doi.org/10.1038/s41467-025-66975-3

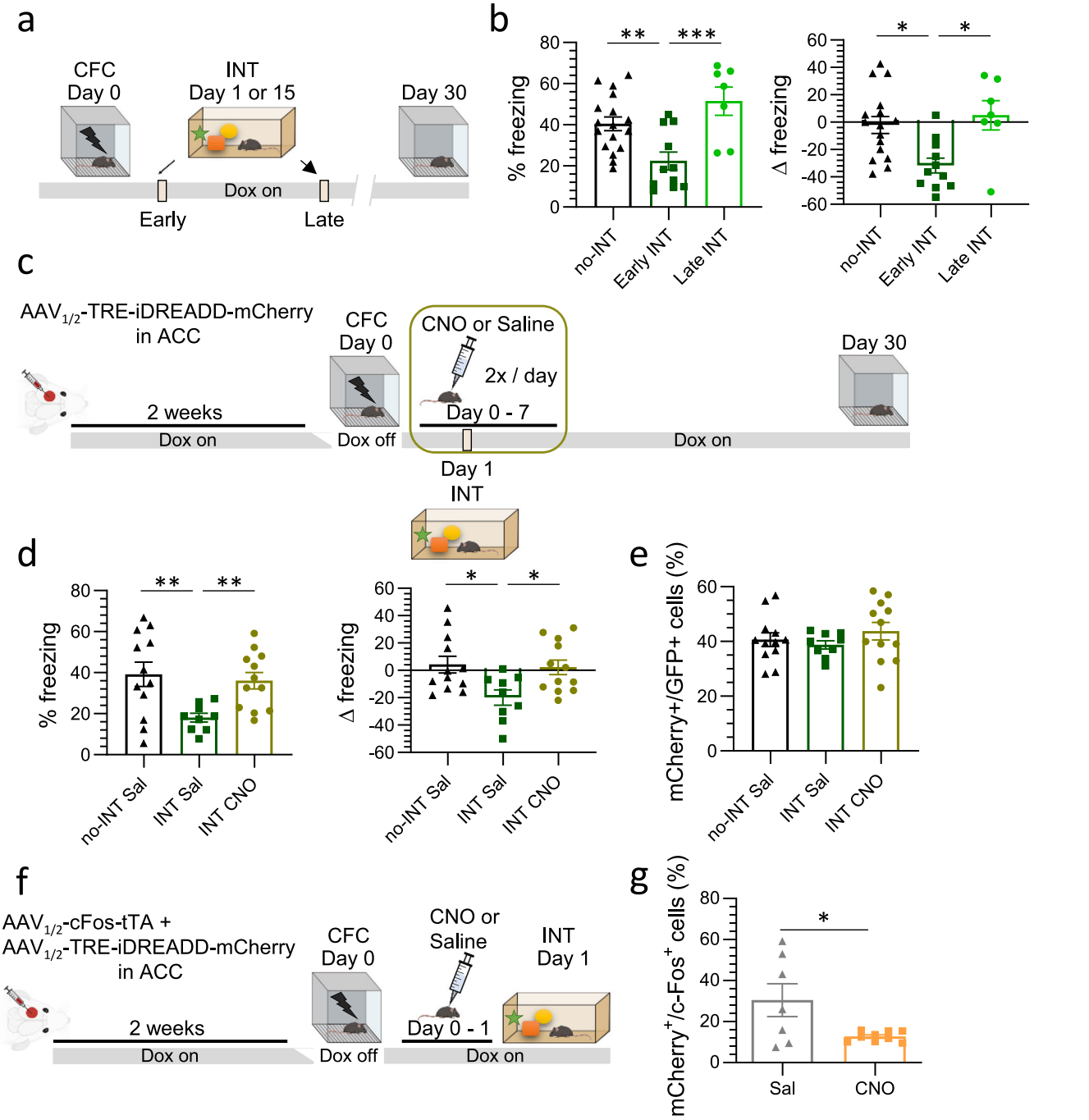

Fig. 5 | Early manipulation of the IE state of ACC engram neurons prevents memory impairment caused by interference. a Experimental design for evaluating remote memory expression following interference (INT, exposure to an enriched environment). Mice underwent INT either one day or 15 days post-CFC. **b** Difference in fear expression between the three groups shows the negative effect of early INT but not late INT on remote memory expression presented as % freezing (no-INT ($n = 17$ mice) vs Early INT ($n = 11$ mice): $t(26) = 3.34$, $p = 0.0025$, CI[-29.14, -6.944], Cohen's $d = 1.28$; early INT vs late INT ($n = 7$ mice): $t(16) = 3.781$, $p = 0.0016$, CI[12.76, 45.34], Cohen's $d = 1.77$) and Δ freezing (no-INT vs Early-INT: $t(26) = 3.38$, $p = 0.0024$, CI[-47.73, -11.60], Cohen's $d = 1.36$; early-INT vs late-INT: $t(16) = 3.371$, $p = 0.0039$, CI[13.63, 59.83], Cohen's $d = 1.30$). **c** Experimental design. Mice from the iDREADD group were injected with CNO for 7 days post-CFC, with INT occurring 24 h following CFC and memory retrieval being tested on day 30. **d** Differences in fear expression: % freezing (no-INT Sal ($n = 12$ mice) vs INT Sal ($n = 9$ mice): $t(19) = 2.94$, $p = 0.0083$, CI[6.113, 36.18], Cohen's $d = 1.38$; INT Sal vs INT CNO ($n = 12$ mice): $t(19) = 3.59$, $p = 0.0020$, CI[-28.59, -7.529], Cohen's $d = 1.66$) and Δ freezing (no-INT Sal vs INT Sal: $t(19) = 2.81$, $p = 0.0112$, CI[6.140 to 42.04], Cohen's $d = 1.26$; INT Sal vs INT CNO: $t(19) = 2.80$, $p = 0.0114$, CI[-38.55, -5.575], Cohen's $d = 1.26$) between the three groups are shown. **e** Percentage of reactivated (mCherry$^+$/GFP$^+$) ACC engram neurons in the same mice during remote memory retrieval shows no difference between groups (no-INT Sal vs INT Sal: $t(19) = 0.56$, $p = 0.5642$, CI[-4.794, 8.529], Cohen's $d = 0.27$; INT Sal vs INT CNO: $t(19) = 1.269$, $p = 0.2197$, CI[-13.12, 3.215], Cohen's $d = 0.59$). **f** Experimental design. Mice expressing iDREADD though viral Tet-Tagging approach ($AAV_{1/2}$-cFos-tTA + $AAV1_{1/2}$-TRE-iDREADD-mCherry) were injected with either Sal or CNO following CFC and 30 minutes prior to INT, and were sacrificed immediately after the INT session. **g** Percentage of reactivated (mCherry$^+$/c-Fos$^+$) ACC engram neurons during INT session was significantly lower in mice injected with CNO compared to Sal (Sal ($n = 7$ mice) vs CNO ($n = 9$ mice): $t(14) = 2.53$, $p = 0.0242$, CI[-32.94, −2.703], Cohen's $d = 1.18$). Means ± SEMs are shown with individual mouse values. Statistical significance was calculated using the two-sided unpaired t-test (b, d, e, g), *p < 0.05, **p < 0.01, ***p < 0.001. See also Supplementary Fig. 11. Created in BioRender. Zhu, L. (2025) https://BioRender.com/jtnacj6 and https://BioRender.com/0uwbq6b.

These results further underline the sensitivity of enduring memory formation to changes in the excitation state of ACC engram ensembles during the early phase of memory consolidation.

Discussion

We present findings showing that neuron-wide IE plasticity constitutes a compelling, necessary, and permissive mechanism for driving the time-dependent process of memory engram reorganization in the neocortex and controlling the informational richness of consolidated engrams. Neuronal allocation has been defined as the selection process that determines which specific neurons become parts of a given memory engram. Neurons exhibiting relatively higher excitability at the time of event encoding predominate in the selection process for engram allocation[20]. In agreement with this concept, we revealed that learning-induced IE plasticity of a set of neurons in the ACC does occur shortly after associative encoding. This form of early neuronal tuning switches their state into a receptive (or "consolidating") mode compatible with information processing and integration. In this mode, ACC engram neurons are more likely to be reactivated by the offline coordinated activity of hippocampal-cortical circuits during periods of quiet wakefulness or phases of sleep[21]. This would promote their permanent integration into the cortical engram by driving persisting changes in synaptic and wiring plasticity[1,22,23], thereby strengthening the connections between nascent engram neurons undergoing consolidation-dependent maturation.

When examining the learning-induced dynamics of IE plasticity, we discovered that the 'tagged' neurons in the ACC not only preferentially matured during the memory consolidation process, leading to their strong recruitment upon remote memory retrieval, but also that their IE underwent neuron-wide plastic modifications that were transient, occurring during the early, but not late, phase of memory onsolidation. How then could this form of cortical IE plasticity contribute to an enduring memory trace [5,6,16]? One possibility is that early neuron-wide IE plasticity primes selected neurons to undergo further plasticity (i.e., metaplasticity[17]), for example, through gene-expression patterns mediated by ion-channel signaling[24], leading to downstream events that reinforce the communication within the nascent engram network. This is consistent with findings of early tagging events in the prefrontal cortex affecting the remote expression of non-aversive memories[5]. In a landscape of increased excitability, synaptic inputs to specific neuronal compartments, such as dendritic branches, could create opportunities for localized persistent excitability plasticity[25–27]. Such localized mechanisms intersect with 'traditional' mechanisms of plasticity, such as long-term potentiation (LTP)[25,28,29], and significantly increase the capacity for storing specific memories[18,30] due to the extended permutations possible with such mechanisms. As a result, changes in IE plasticity elicited by an associative learning episode could modulate the threshold for induction of an online wave of LTP in the synapses of allocated ACC neurons, which in turn contributes to establishing the selectivity of their neuronal firing to an aversive context, as previously reported for the hippocampus[31]. Another way that neuron-wide IE plasticity could contribute during the early consolidation period is to set the stage for synapse-specific tuning by eliciting changes in the intracellular localization and targeting of ion channel complexes. Such changes are known to occur during development[32] or pathophysiological states (Kv2.1 and epilepsy[33]), and are often due to the association of pore-forming subunits of an ion channel with accessory subunits that confer properties of localization. The IE plasticity changes reported here are likely due to the orchestrated effect of a spectrum of different ion channel types (notably Na^+, Ca^{2+}, and K^+ channels), and many of these are susceptible to modulatory processes, such as phosphorylation or association with accessory subunits that affect their properties[34]. A finer-grained form of plasticity, operating at the nuclear level, namely chromatin plasticity, has recently been revealed as a mechanism coordinating which neurons are eligible for inclusion into the memory engram[35]. Interestingly, chromatin plasticity has been found to act on IE and synaptic remodeling of neuronal ensembles in a cell-intrinsic manner, thus pointing to IE plasticity as a transducer between the epigenetic state of a neuron and its trajectory towards preferential selection for enduring storage of learned information. Notably, these two complementary forms of plasticity were triggered using aversive memory paradigms, such as Pavlovian fear learning[35] and here, CFC. Whether their involvement in remote memory formation is generalizable to other types of non-aversive learning (e.g., spatial or associative) remains to be formally tested. That early tagging of certain cortical neurons with epigenetic marks upon encoding of associative olfactory memory is a prerequisite for the formation of enduring memories[5] suggests that it may well be the case.

By artificially manipulating the excitation state in those ACC neurons initially tagged during the learning event (nascent engram neurons), we established the necessity of precocious, but not late, cortical IE plasticity for recruiting nascent cortical memory engram cells and for initiating their subsequent maturation and stabilization. Thus, IE plasticity appears no longer required once the physical and chemical engram alterations underlying permanent memory storage have been established, further supporting the assumption that this form of plasticity cannot endorse the role of a permanent memory storage mechanism since it would severely lower the storage capacity of neurons compared to one where information is stored in a synapse-specific manner[5,18]. Functionally, such a time-limited tuning of the neuron-wide IE plasticity may serve as a key gateway for triggering early offline LTP as well as the additional waves of synaptic plasticity events recently identified as prerequisites for systems consolidation[31]. Surprisingly, early iDREADD-mediated hyperpolarization, but not eDREADD-induced depolarization, of tagged ACC engram ensembles was beneficial for remote memory formation (enhanced consolidation) and for improving context discrimination (more richly detailed informational content). Off-target clozapine effects cannot be entirely ruled out, but the low CNO dose (5 mg/kg), bidirectional iDREADD/eDREADD responses, lack of CNO effects at remote phases, and a 1–3-week washout collectively make this unlikely.

We pinpointed changes in the excitability of neurons in layer 5 of the ACC engram network, but other cortical layers or neuron types, including various interneuron types, are also likely targeted by our "tet-tagging" strategy. Thus, interventions targeting the excitation of the overall ACC engrams could have outcomes that might seem counterintuitive at first consideration but are consistent with the notion of this heterogeneity. The most parsimonious explanation for the unexpected beneficial effect of iDREADD manipulation is that hyperpolarization could restrict the competitive advantage of dominant ACC engram neurons, which is derived from their heightened responsiveness due to increased excitability. Tilting the balance toward non-engram cells would hinder the preferential activation of dominant fear engram cells by new oncoming experiences and impede their reallocation to other neuronal ensembles (as shown in our study), thereby maintaining their initial context-specific memory content as consolidation proceeds. In this way, IE plasticity would act as an essential gating mechanism ensuring the embedding of encoding specificity within the boundaries of the cortical engram network initially allocated to the encoded memory. Fear generalization to irrelevant contexts would then be minimized by authorizing the allocation of other non-engram cells to novel context associations, whether similar or conflicting[36].

The operating features of cortical IE plasticity we uncovered have functional implications for consolidation-based processes. First, IE plasticity controls the informational content (or precision) of remote memories, which we addressed by challenging mice with different contexts upon remote memory retrieval. Promoting the reactivation of only those memories that are the most relevant for the context at hand

has been conceptualized in the form of a hippocampal index embedded precociously within the initially tagged engram network that would aid in coordinating memory retrieval[37]. Since the ACC constitutes a central hub within the set of interconnected cortical regions supporting remote memory[7], it stands as a likely candidate for potentially hosting an equivalent, or complementary cortically-based index, which could rely on IE plasticity as its main supportive mechanism. In this view, the IE plasticity gating mechanism would support an inherent cortical system for integrating the richly detailed content of cortical memories being processed until their stabilization.

Second, IE plasticity enables cortically-maturing engrams to cope with oncoming interfering events. Experiencing a second proximate event can disrupt the consolidation of a first one (retrospective interference), possibly by reversing learning-induced LTP, resulting in memory forgetting[38]. Concurring with this, we impaired remote memory retrieval when administering retroactively an interfering event during the early phase of memory consolidation. Pharmacogenetic hyperpolarization of ACC engram neurons rescued this deficit, likely by preventing their reallocation into the new interfering engram network, as suggested by our data. Consolidated memory engrams are not acquired inflexibly but are thought to reorganize over time to enable linkage or inferences across separate or related experiential events[39]. Such malleability suggests overlapping of neuronal ensembles representing multiple contextual memories, a process during which IE plasticity could play a key role, notably in ensuring parallel processing while preventing catastrophic interferences. For instance, IE plasticity could contribute to the synaptic rearrangement of GluN2B-containing N-methyl-d-aspartate (NMDA) receptors, which was recently proposed to dictate the progressive embedding of enduring engrams in the cortex and control their malleability[40].

Third, the restricted temporal dynamics of neuron-wide IE plasticity during systems consolidation point to a division of labor between complementary mechanisms supporting memory integration and enduring storage. The observation that tampering with the engram excitation during the late phase of systems consolidation did not impact remote memory retrieval indicates that additional mechanisms, such as synaptic plasticity and rewiring as well as dendritic branch-specific IE plasticity[26,27], take place to ensure the full maturation of cortical engram cells, including their well-organized synaptic architecture and connectivity within the engram cell network. It is reasonable to assume that it is only under this late storage configuration that enduring cortical memory engrams will express their full vividness upon retrieval.

Here, we unraveled the dynamics of IE plasticity and its operating features in configuring cortical engram neurons, highlighting its crucial role in determining the fate and informational content of remote, consolidated contextual fear memories. We focused on the ACC, but remote memories are embedded within a distributed cortical network involving multiple interconnected sensory, motor, and limbic cortices[2,41–43]. This raises the possibility that other distributed neurons in the orbitofrontal, prefrontal (e.g., prelimbic and infralimbic cortex, reviewed in ref. 14), parietal and retrosplenial cortices conjointly undergo IE changes, albeit possibly through different operational temporal dynamics. Our study proves that modulating the IE state during its plastic phase renders nascent engram neurons resilient to interference, ensuring their successful maturation as cortical engram neurons. Investigating whether these mechanisms are equally advantageous in counteracting memory forgetting over time by preventing cortical engrams from undergoing de-maturation (resulting in retrieval failure or memory erasure) would be highly relevant in physiology and physiopathology. We show that IE plasticity constitutes a necessary, permissive step of memory engram formation, suggesting that IE, synaptic plasticity, and synaptic reorganization mechanisms are intricately related during the formation of enduring cortical engrams. These complementary mechanisms likely cooperate to ensure the malleable nature and physical manifestation of cortical engrams, and future efforts should be devoted to understanding how novel information can be incorporated into non-naive neuronal networks already hosting pre-existing engrams or associative neocortical mental schemas[44].

Methods

Animals

Double transgenic Tet-Tag mice (Fos-tTA and Fos-EGFP; tetO-lacZ and tTA*) on C57BL/6 x DBA/2 background (Jax# 008344) were used for all the experiments that required long-term labeling of putative engram neurons: electrophysiological, DREADD, and interference experiments (combined with remote memory retrieval). Single transgenic mice (Fos-tTA/Fos-EGFP) were used for the rest of the experiments. 380 adult mice of both sexes were used for all the behavioral and electrophysiological experiments. As we observed no sex differences in our measures, data from both genders were pooled. Mice were stereotaxically injected at 6–12 weeks of age and tested at 8–16 weeks of age. Mice were bred in the animal facility of the Neurocentre Magendie, group-housed, and kept at a 12-hour light-dark cycle (light on from 7 am to 7 pm) in temperature (22 °C ± 1 °C) and humidity (55% ± 10%) controlled rooms and with *ad libitum* access to water and doxycycline chow (40 mg/kg). Doxycycline chow was replaced with standard chow (no doxycycline) 48 h before fear conditioning to open the temporal window for tagging and provided back immediately following the learning experience.

Viral constructs and stereotaxic surgeries

Two weeks before CFC, the ACC area of Tet-Tag mice was stereotactically injected with either one of the adeno-associated viruses (AAVs), AAV1/2-TRE-hM$_3$Dq-mCherry, AAV1/2-TRE-hM$_4$Di-mCherry, AAV1/2-TRE-YFP or with a combination of AAV1/2-c-Fos-tTA and AAV1/2-TRE-hM$_4$Di-mCherry at a 1:1 ratio (for single transgenic Fos-EGFP mice). AAV1/2-TRE-hM4Di-mCherry was created by cloning hM4D(Gi)-mCherry (Addgene #50475) into pAAV-PTRE-tight-hM3Dq-mCherry (Addgene #66795). AAV1/2-c-Fos-tTA was obtained from Addgene (Plasmid #66794). AAV1/2-TRE-YFP was provided by Dr. Tonegawa (MIT)[45].

Thirty minutes before the surgery, mice received a subcutaneous injection of the analgesic buprenorphine solution (0.1 mg/kg, AXIENCE SAS). Mice were then deeply anesthetized with 4% isoflurane, placed in a stereotaxic frame, then switched to 2% isoflurane for the rest of the surgery. Before incising the skin on the skull, mice received a subcutaneous injection of a local anesthetic, lidocaine (0.1 mg/ml, AXIENCE SAS; 0.05–0.1 ml), at the site of the incision. Surgery commenced once the mice displayed no reflexes after paw pinch. Bilateral stereotaxic infusions of the AAV were targeted to the ACC using the following coordinates (relative to bregma) and infusion angle: AP + 0.9 mm, ML ± 0.75 mm, DV -1.65 mm, 20° from a vertical line. Five hundred nl of AAV virus was infused into each site at a rate of 100 nl/min. The needle was slowly removed 5 min after completion of the infusion. Mice were given a two-week post-surgery recovery period before starting experiments. Active AAV particles were either produced in-house, or by the AAV facility of the Bordeaux Neurocampus. Titration was performed by the transcription platform of the Neurocentre Magendie.

Behavioral testing

Contextual fear conditioning (CFC). Before behavioral training, mice were habituated in a waiting room and handled daily (10–20 min) for five consecutive days. CFC consisted of a 3 min free-exploring phase of the conditioning chamber by each mouse (context A, scented with 70% ethanol), followed by five 2 s-long foot shocks (intensity 0.7 mA) with a shock interval of 30 s. Context A was a gray plastic chamber (Supplementary Table 4; 26 cm long, 25 cm in-depth, 18 cm in height,

Imetronic, Marcheprime, France) with a metal grid floor to deliver electric shocks and a transparent Perspex door. After the shocks, the animals remained in the chamber for another 30 seconds. A control group (CTX) was exposed to context A, also scented with 70% ethanol, for the same amount of time (five minutes and 40 seconds in total) but without receiving any foot shocks. For memory retrieval, mice were re-exposed to the conditioning chamber (context A) for 3 min without receiving foot shocks or to context B (chamber with an additional white, prism-like box with a plastic floor that was shaped like a triangle and contained no metal grids) in the same room (see Supplementary Table 4 for detailed comparison of contexts A and B). To evaluate the strength of fear memory during different temporal phases of memory formation, we assessed the freezing time of each mouse in a given context (A or B). Freezing behavior was considered as the absence of any movement, except for respiratory-related movement.

Freezing time during memory recall was manually counted by two independent experimenters who were blind to the experimental conditions. The percentage of freezing was calculated as the measured freezing time divided by the three minutes of the retrieval period. We also calculated the freezing time during the 30 s that followed the last shock of CFC (% freezing after learning) as the basal freezing level for every mouse. Delta freezing (Δ freezing) was calculated as follows: Δ freezing = (% freezing during retrieval) − (% freezing after learning).

Pharmacogenetic manipulation. To modulate the excitation state of neuronal ACC engram ensembles transduced with AAV1/2-TRE-hM$_3$Dq-mCherry (excitatory DREADD, eDREADD) or AAV1/2-TRE-hM$_4$Di-mCherry (inhibitory DREADD, iDREADD), mice received Clozapine-N-oxide (CNO) or vehicle (saline, Sal) via intraperitoneal (*i.p.*) injection twice a day. To modulate the excitability during the early stages of memory consolidation, the first CNO/Sal *i.p.* injection was administered 6 hours after the CFC and continued daily for the subsequent seven days. To alter the excitability of engram neuron ensembles during the late memory consolidation, mice received the first CNO/Sal *i.p.* injection on day 15 after the CFC and then for the following seven consecutive days (until day 22 following CFC). Injections were delivered between 9 and 10 a.m. and 3 and 4 p.m. on a given day. Mice were returned to their home cages immediately after each *i.p.* injection.

CNO (TOCRIS) was dissolved in DMSO (Sigma-Aldrich) at a stock concentration of 5 mg/ml and stored at -20°C. Aliquots of CNO stock solution were thawed before the injections and diluted to a final concentration of 0.5 mg/ml with a 0.9% NaCl solution. DMSO was diluted in the same manner and served as control (vehicle). CNO (or vehicle) was injected *i.p.* at 5 mg/kg body weight.

We verified the expression of the DREADD receptors within the ACC area of interest by imaging mCherry$^+$ neurons in brain slices using confocal microscopy (described below). Only mice with mCherry expression circumscribed to the appropriate ACC area were considered for histological, behavioral, and statistical analyses.

Memory interference protocol. On day 1 (early memory interference, early-INT) or day 15 (late memory interference, late-INT) following CFC, mice were either allowed to explore a novel environment for two hours (interference group) or stayed in their home cage (no-interference control group). This novel environment consisted of a cage twice the size of the home cage, covered with black paper, with only one transparent side to see the distal cues on the wall. Toys were placed inside the cage and rearranged every 20 minutes to stimulate exploratory behavior. In addition, mice had access to a running wheel for an hour. Water and doxycycline food was available for the duration of the whole experiment. The influence of interference on memory recall was assessed 30 days after CFC by placing mice in the same context where they were conditioned (context A) for 3 minutes.

To probe how pharmacogenetic hyperpolarization of ACC engram neurons alters the interference-induced impairment of memory formation, animals were injected with AAV1/2-TRE-hM$_4$Di-mCherry into the ACC two weeks before CFC. Mice of the interference group were randomly divided into two subgroups, one receiving *i.p.* CNO injections and the other *i.p.* vehicle injections for seven days each during either the early or late phase of memory consolidation (see above). The no-interference control group received vehicle injections during the same 7-day period and stayed in their home cage. Memory retrieval was performed for all three groups 30 days after CFC in Context A. A separate group of mice that received CNO or saline twice (6 h after CFC and 30 min before INT the next day) was sacrificed following INT, without a retrieval session, to assess re-allocation of CFC-associated engram neurons.

Electrophysiology

ACC slice preparation. Mice were sacrificed for electrophysiological recordings 1–3 days, 8–9 days or 15–17 days following the behavioral session (CFC or CTX) without memory recall. Mice were deeply anesthetized with isoflurane, and intracardially perfused with ice-cold (4 °C) cutting solution (for composition, see Supplementary Table 5) once the mice displayed no reflexes after paw pinch. Following the perfusion, mice were decapitated, their heads were immersed in the ice-cold cutting solution, and the brains were rapidly removed. Coronal slices of 300 μm were cut using a vibratome (Vibratome 3000 Plus, Sectioning Systems) and gently transferred to an incubating chamber filled with artificial cerebrospinal fluid (aCSF) resting solution (Supplementary Table 5). Following 40 min of incubation at 37 °C, slices were transferred to a second incubation chamber containing aCSF recording solution at room temperature (~ 23 °C) (Supplementary Table 5). Brain slices were allowed to recover for at least one hour before electrophysiology recordings. All the solutions were saturated with carbogen (95% O_2, 5% CO_2), the pH adjusted to 7.32–7.40, and the osmolarity adjusted to 295–310 mOsm.

Whole-cell patch-clamp recordings. Following the behavioral protocol, mice aged 8–16 weeks were randomly assigned to the 1-3-day, 8-9-day and 15-17-day groups for electrophysiological experiments (age in weeks, CTX D1-3: 12.59 ± 1.16, $n = 9$; CTX D8-9: 13.14 ± 0.68, $n = 5$; CTX D15-17: 12.64 ± 0.65, $n = 9$; CFC D1-3: 12.97 ± 1.12, $n = 8$; CFC D8-9: 10.94 ± 0,83, $n = 5$ CFC D15-17: 13.24 ± 0,68, $n = 11$; no age difference). Layer 5 thick-tufted pyramidal neurons within acute ACC slices were selected for whole-cell recordings using an upright microscope (Zeiss Examiner) equipped with a 63X/1.0 NA water immersion objective (Zeiss) and an IR-Dodt contrast system. An Evolve 512 EMCCD Camera (Photometrics) combined with an LED system (560 nm; Colibri, Zeiss) and a Filter Set 62 HE (Zeiss) was used for visualizing YFP-expressing putative ACC engram neurons. For whole-cell recordings, borosilicate glass capillaries (Harvard Instruments, GC150F-7.5) were pulled using a PC-100 vertical puller (NARISHIGE Group). The pipettes were filled with internal recording solution (Supplementary Table 5), and the open-tip resistance ranged from 5 to 7 MΩ. The osmolarity of the internal solution containing 0.3% biocytin (Reference: 90055, Biotium) was adjusted to 290 mOsm, and the pH was set to 7.30. The solution was stored at -20 °C and kept on ice before use. The recording chamber of the electrophysiology setup was perfused with oxygenated aCSF at a temperature of 32 °C during the whole experiment.

Recordings were performed in the bridge mode using a BVA-700C (Dagan, USA) and MultiClamp 700B amplifier (Molecular Devices, Sunnyvale, CA). Data were low-pass filtered at 3 kHz and sampled at 20 kHz using an ITC-18 (InstruTECH) Data Acquisition Interface and AxoGraph X software (version 1.7.6), or a Digidata 1550 computer interface with PClamp11 software (MolecularDevices). Bridge resistance and capacitance were compensated and monitored during the recording period. Cells were discarded if the resting membrane potential was depolarized above -50 mV. All electrophysiological properties were measured in the bridge-mode.

To measure the intrinsic properties of ACC neurons, recordings were performed in the presence of the following blockers of glutamatergic and GABAergic synaptic transmission: AMPA receptor antagonist, NBQX (disodium salt, TOCRIS; concentration: 3 µM in aCSF), NMDA receptor antagonist, DL-AP5 (TOCRIS; 50 µM), and $GABA_A$ receptor antagonist, SR 95531 (hydrobromide, TOCRIS; 10 µM).

Morphological reconstruction of recorded neurons. After electrophysiological recordings, the brain slices containing the biocytin-filled recorded neurons were fixed in 4% PFA for two hours and then transferred to 0.1 M PBS solution at 4 °C. Brain slices were washed three times with 0.1 M PBS and then submerged for two hours at room temperature with a 0.7% Triton X-100 solution (EUROMEDEX). Slices were then incubated with a solution that contained Streptavidin-Alexa 555 (1:1000, Thermo Fisher, Reference: S21318) and 0.3% Triton X-100 for three hours. The brain slices were then washed with 0.1 M PBS three times and incubated with DAPI (1:10000, Sigma-Aldrich) for five minutes. Brain slices were mounted on microscope slides using Mowiol-Dabco and thin coverslips.

Confocal microscopy was used to image the recorded neurons (YFP^+/Alexa 555^+ neurons). The distances of the recorded neurons to the pia and the beginning of layer 2 were also measured to define the layer localization of the neurons. The morphology of soma and dendrites was reconstructed with Neurolucida software, and only *post hoc* identified layer 5 tick-tufted pyramidal neurons were included for analysis.

Electrophysiological data analysis. Electrophysiological data were analyzed using AxoGraph X, PClamp11, and customized Python analysis routines. The resting membrane potential (RMP) was measured 3 minutes after whole-cell access and switching to the bridge mode to allow for the cells to stabilize. The input resistance was measured as the average (five trials) steady-state voltage deflection to a -20 pA current step (800 ms duration). Rheobase and the number of action potentials (AP) as a function of current were determined by injecting a series of depolarizing current steps of increasing amplitude (between 0 and 300 pA, 20 pA increments, 800 ms duration). The rheobase was defined as the minimum amount of current necessary to evoke the first AP. The first AP within a train of 4-5 APs was analyzed for AP threshold (dV/dt exceeding 10 mV/ms, in mV), AP amplitude (from RMP to peak amplitude, mV), AP half-width (duration at half-distance between AP threshold and amplitude, ms), and maximum rate of rise (dV/dt, mV/ms). The inter-spike interval (ISI, AP adaptation, ms) was measured between the first two and the last two APs within a train of 4 - 5 APs, and the AP adaptation index was measured as follows: (first ISI) / (last ISI). The membrane time constant (ms) was calculated from voltage responses to alternating depolarizing and hyperpolarizing 400 pA 1-ms-long current pulses. It was then calculated as the slow component of a double-exponential fit of the average voltage decay in both the depolarizing and hyperpolarizing directions. The medium afterhyperpolarization (mAHP) was measured as the minimum (relative to RMP) 50–100 ms following the last AP within a train of 5 APs (2 ms pulses, 2 nA) evoked at frequencies ranging from 20 to 120 Hz (at 20 Hz intervals), and 200 Hz.

Immunohistochemistry and imaging

Sacrifice and slice preparation. Ninety minutes after the behavior (CFC) or following the INT, mice were deeply anesthetized by 4% isoflurane and *i.p.* injected with a solution containing 400 mg/ml of pentobarbital (Exagon, Med'Vet) and 0.1 mg/ml of lidocaine (Lidor, AXIENCE SAS) in a 0.9% NaCl solution. The injection dose was 0.1 ml/10 g of mouse body weight. Mice were then transcardially perfused with 0.1 M phosphate-buffered saline (PBS) followed by 4% cold paraformaldehyde (PFA). Mice of the HC group, which did not undergo any behavioral procedure, were perfused on the same day. Brains were dissected and postfixed overnight in 4% paraformaldehyde, then sliced into 50 µm coronal sections using a vibratome.

Immunohistochemistry staining. Brain slices were washed three times with 0.1 M PBS for 10 minutes each, and then blocked for one hour at room temperature with the following blocking solution: 5% BSA (EUROMEDEX) mixed with 0.3% Triton X-100 (EUROMEDEX). To enhance the GFP signal, slices were incubated with anti-GFP rabbit polyclonal antibody Alexa-488 (1:1000, Thermo Fisher, Reference: A21311) overnight at 4 °C in a solution containing 1% BSA and 0.3% Triton X-100. To label c-Fos^+ and $parvalbumin^+$ neurons, slices were incubated with anti-c-Fos (9F6) rabbit monoclonal antibody (1:1000, Cell Signaling) or anti-Parvalbumin (PV) mouse monoclonal antibody (1:1000, Merck Reference: SAB4200545), respectively, under the same condition. The following day, slices were washed three times with 0.1 M PBS for 10 minutes each and secondary goat anti-rabbit Alexa fluor 647 antibody (1:2000, Thermo Fisher, Reference: A21244) and goat anti-mouse Alexa fluor 647 (1:2000, Thermo Fisher, Reference: A32728) was added, respectively, and slices were incubated with DAPI (1:10000, Sigma-Aldrich) for 5 min. After being washed once with 0.1 M PBS, the brain slices were mounted using Mowiol-Dabco and thin coverslips on microscope slides.

Confocal image acquisition and analysis. Fluorescence images were acquired using a Zeiss LSM700 confocal microscope equipped with a Leica 20X/1.3 NA oil immersion lens provided by the Bordeaux Imaging Center (BIC). Two to three coronal slices per mouse were imaged at multiple depths along the z-axis (z-stack of 32 µm with 4 µm interval steps). Imaris software (version 9.6.2) enabled the reconstruction of a 3-dimensional model from confocal microscopy images. Cell counting analysis was performed using Imaris and ImageJ-Fiji software (provided by BIC). The area of the ACC was selected and measured with ImageJ-Fiji. The number (#) of $mCherry^+$, GFP^+, c-Fos^+, PV^+ and/or co-localized ($mCherry^+$/GFP^+, $mCherry^+$/c-Fos^+, or $mCherry^+$/PV^+), and $DAPI^+$ neurons were counted and expressed as cell density per mm^2 ((#cells/area size (μm^2)) x 1000000). To account for differences in the total number of $mCherry^+$ cells between conditions, colocalization was expressed as the percentage of $mCherry^+$ cells that were also GFP^+/c-Fos^+, calculated as follows:

$mCherry^+/GFP^+$ cells (%) = (# $mCherry^+/GFP^+$ cells)/(# $mCherry^+$ cells) × 100 or $mCherry^+$/c-Fos^+ cells (%) = (# $mCherry^+$/c-Fos^+ cells)/(# $mCherry^+$ cells) × 100 or $mCherry^+/PV^+$ cells (%) = (# $mCherry^+/PV^+$ cells)/(# $mCherry^+$ cells) × 100.

Image acquisition and analysis were performed blind to the experimental conditions.

Statistics and Reproducibility. Statistical tests were performed using Prism 10.0 (GraphPad) and Social Science Statistic (https://www.socscistatistics.com/) platform. No statistical methods were used to predetermine sample size, but the number of animals used in each experiment was based on previous work of a similar nature by our laboratory[46]. Animals were randomly allocated to the different experimental groups without using a specific randomization method. Normality of data distribution was verified using the Shapiro–Wilk test. Two-sided Student's unpaired t-test or Mann–Whitney U test was used to examine statistical difference between two groups. The significance of the difference among multiple groups was calculated by one-way and two-way ANOVA (with repeated measures where necessary), followed by an appropriate post hoc test when significant main effects or interactions were detected. Where applicable, effect sizes were reported as Cohen's d for pairwise comparisons and partial eta squared (η^2) for ANOVA analyses, to provide an estimate of the magnitude of observed effects. A 95% confidence interval (CI) of the mean was reported for all parametric analyses where available. Unpaired t-tests or Mann–Whitney U tests were used to compare

control (CTX-YFP$^+$) and test (CFC-YFP$^+$) groups within two time points in the electrophysiological recordings. To correct for multiple comparisons, the two-stage step-up method of Benjamini, Krieger and Yekutieli was applied to control the false discovery rate (FDR; reported as q values). Temporal comparisons (early vs. late) were performed on CFC values normalized to their respective controls using unpaired t-tests. The sample sizes and statistical analysis details are reported in each figure legends. Electrophysiological recordings were conducted across multiple independent batches of mice (biological replicates) to ensure reproducibility. Behavioral experiments, including pharmacogenetic interventions, were replicated across a minimum of two independent cohorts. The Dox ON control condition, implemented to verify the absence of neuronal tagging, was assessed in three mice.

Source data are provided as a Source Data file. Schematic of the mouse was taken from BioRender.com.

Data were displayed as mean ± SEM. The significance threshold was set at $\alpha = 0.05$ ($^{*}p < 0.05$, $^{**}p < 0.01$, $^{***}p < 0.001$, $^{****}p < 0.0001$, $^{\S}p < 0.05$, $^{\S\S}p < 0.01$, $^{\S\S\S}p < 0.001$ for interaction effect).

Ethical considerations

All animal procedures, including anesthesia and surgery, conformed with European law (Directive 2010/63/EU). The experiments were approved by the Bordeaux Ethics Committee (CEEA50) and the Ministry of Higher Education and Research (MESRI). The ethics protocol numbers allocated to these experiments were 9000,12267, 51163, and 51164.

Reporting summary

Further information on research design is available in the Nature Portfolio Reporting Summary linked to this article.

Data availability

Source data are provided as a Source Data file. The electrophysiological recordings data generated in this study have been deposited in the Figshare repository: https://doi.org/10.6084/m9.figshare.30620135.v4 Source data are provided with this paper.

Code availability

Custom code for electrophysiological analysis is available on GitHub (https://github.com/Yves33/Intrinsic/).

References

1. de Sousa, A. F. et al. Optogenetic reactivation of memory ensembles in the retrosplenial cortex induces systems consolidation. *Proc. Natl. Acad. Sci. USA* **116**, 8576–8581 (2019).
2. Frankland, P. W. & Bontempi, B. The organization of recent and remote memories. *Nat. Rev. Neurosci.* **6**, 119–130 (2005).
3. Bero, A. W. et al. Early remodeling of the neocortex upon episodic memory encoding. *Proc. Natl. Acad. Sci.* **111**, 11852–11857 (2014).
4. Kitamura, T. Driving and regulating temporal association learning coordinated by entorhinal-hippocampal network. *Neurosci. Res.* **121**, 1–6 (2017).
5. Lesburguères, E. et al. Early tagging of cortical networks is required for the formation of enduring associative memory. *Science* **331**, 924 LP–924928 (2011).
6. Roy, D. S. et al. Brain-wide mapping reveals that engrams for a single memory are distributed across multiple brain regions. *Nat. Commun.* **13**, 1799 (2022).
7. Frankland, P. W., Bontempi, B., Talton, L. E., Kaczmarek, L. & Silva, A. J. The Involvement Of The Anterior Cingulate Cortex In Remote Contextual Fear Memory. *Science* **304**, 881 LP–881883 (2004).
8. Tayler, K. K., Tanaka, K. Z., Reijmers, L. G. & Wiltgen, B. J. Reactivation of neural ensembles during the retrieval of recent and remote memory. *Curr. Biol.* **23**, 99–106 (2013).
9. Cai, D. J. et al. A shared neural ensemble links distinct contextual memories encoded close in time. *Nature* **534**, 115–118 (2016).
10. Rashid, A. J. et al. Competition between engrams influences fear memory formation and recall. *Science* **353**, 383–387 (2016).
11. Frick, A. & Johnston, D. Plasticity of dendritic excitability. *J. Neurobiol.* **64**, 100–115 (2005).
12. Titley, H. K. et al. Intrinsic excitability increase in cerebellar Purkinje cells after delay eye-blink conditioning in mice. *J. Neurosci.* **40**, 2038–2046 (2020).
13. Zhang, W. & Linden, D. J. The other side of the engram: experience-driven changes in neuronal intrinsic excitability. *Nat. Rev. Neurosci.* **4**, 885–900 (2003).
14. Yousuf, H., Ehlers, V. L., Sehgal, M., Song, C. & Moyer, J. R. Modulation of intrinsic excitability as a function of learning within the fear conditioning circuit. *Neurobiol. Learn. Mem.* **167**, 107132 (2020).
15. Abraham, W. C., Jones, O. D. & Glanzman, D. L. Is plasticity of synapses the mechanism of long-term memory storage? *npj Sci. Learn.* **4**, 1–10 (2019).
16. Takeuchi, T., Duszkiewicz, A. J. & Morris, R. G. M. The synaptic plasticity and memory hypothesis: encoding, storage and persistence. *Philos. Trans. R. Soc. B Biol. Sci.* **369**, 20130288 (2014).
17. Hansel, C. & Yuste, R. Neural ensembles: role of intrinsic excitability and its plasticity. *Front. Cell. Neurosci.* **18**, 1440588 (2024).
18. Poirazi, P. & Mel, B. W. Impact of active dendrites and structural plasticity on the memory capacity of neural tissue. *Neuron* **29**, 779–796 (2001).
19. Dixsaut, L. & Gräff, J. The medial prefrontal cortex and fear memory: dynamics, connectivity, and engrams. *Int. J. Mol. Sci.* **22**, 12113 (2021).
20. Josselyn, S. A. & Frankland, P. W. Memory allocation: mechanisms and function. *Annu. Rev. Neurosci.* **41**, 389–413 (2018).
21. Rusu, S. I. et al. Offline orbitofrontal cortex reactivation depends on recency of place-reward changes and coheres with hippocampal replay. *iScience* **27**, 109205 (2024).
22. Diekelmann, S. & Born, J. The memory function of sleep. *Nat. Rev. Neurosci.* **11**, 114–126 (2010).
23. Girardeau, G. & Zugaro, M. Hippocampal ripples and memory consolidation. *Curr. Opin. Neurobiol.* **21**, 452–459 (2011).
24. Vierra, N. C., O'Dwyer, S. C., Matsumoto, C., Santana, L. F. & Trimmer, J. S. Regulation of neuronal excitation-transcription coupling by Kv2.1-induced clustering of somatic L-type Ca2+ channels at ER-PM junctions. *Proc. Natl. Acad. Sci. USA* **118**, e2110094118 (2021).
25. Frick, A., Magee, J. & Johnston, D. LTP is accompanied by an enhanced local excitability of pyramidal neuron dendrites. *Nat. Neurosci.* **7**, 126–135 (2004).
26. Makara, J. K. & Magee, J. C. Variable dendritic integration in hippocampal CA3 pyramidal neurons. *Neuron* **80**, 1438–1450 (2013).
27. Schreurs, B. G., Gusev, P. A., Tomsic, D., Alkon, D. L. & Shi, T. Intracellular correlates of acquisition and long-term memory of classical conditioning in Purkinje cell dendrites in slices of rabbit cerebellar lobule HVI. *J. Neurosci.* **18**, 5498–5507 (1998).
28. Rosenkranz, J. A., Frick, A. & Johnston, D. Kinase-dependent modification of dendritic excitability after long-term potentiation. *J. Physiol.* **587**, 115–125 (2009).
29. Lin, T.-F., Busch, S. E. & Hansel, C. Intrinsic and synaptic determinants of receptive field plasticity in Purkinje cells of the mouse cerebellum. *Nat. Commun.* **15**, 4645 (2024).
30. Häusser, M. Storing memories in dendritic channels. *Nat. Neurosci.* **7**, 98–100 (2004).
31. Goto, A. et al. Stepwise synaptic plasticity events drive the early phase of memory consolidation. *Science* **374**, 857–863 (2021).
32. Wilkars, W. et al. Regulation of axonal HCN1 trafficking in perforant path involves expression of specific TRIP8b isoforms. *PloS One* **7**, e32181 (2012).

33. Thiffault, I. et al. A novel epileptic encephalopathy mutation in KCNB1 disrupts Kv2.1 ion selectivity, expression, and localization. *J. Gen. Physiol.* **146**, 399–410 (2015).
34. Misonou, H. et al. Regulation of ion channel localization and phosphorylation by neuronal activity. *Nat. Neurosci.* **7**, 711–718 (2004).
35. Santoni, G. et al. Chromatin plasticity predetermines neuronal eligibility for memory trace formation. *Science* **385**, eadg9982 (2024).
36. Cui, K. et al. Dominant activities of fear engram cells in the dorsal dentate gyrus underlie fear generalization in mice. *PLoS Biol.* **22**, e3002679 (2024).
37. Coelho, C. A. O. et al. Dentate gyrus ensembles gate context-dependent neural states and memory retrieval. *Sci. Adv.* **10**, eadn9815 (2024).
38. Ge, M. et al. Memory Susceptibility to Retroactive Interference Is Developmentally Regulated by NMDA Receptors. *Cell Rep.* **26**, 2052–2063.e4 (2019).
39. Zaki, Y. & Cai, D. J. Memory engram stability and flexibility. *Neuropsychopharmacology* **50**, 285–293 (2025).
40. Bessières, B., Dupuis, J., Groc, L., Bontempi, B. & Nicole, O. Synaptic rearrangement of NMDA receptors controls memory engram formation and malleability in the cortex. *Sci. Adv.* **10**, eado1148 (2024).
41. Takehara, K., Kawahara, S. & Kirino, Y. Time-dependent reorganization of the brain components underlying memory retention in trace eyeblink conditioning. *J. Soc. Neurosci.* **23**, 9897–9905 (2003).
42. Maviel, T., Durkin, T. P., Menzaghi, F. & Bontempi, B. Sites of neocortical reorganization critical for remote spatial memory. *Science* **305**, 96–99 (2004).
43. Teixeira, C. M., Pomedli, S. R., Maei, H. R., Kee, N. & Frankland, P. W. Involvement of the anterior cingulate cortex in the expression of remote spatial memory. *J. Soc. Neurosci.* **26**, 7555–7564 (2006).
44. Tse, D. et al. Schemas and memory consolidation. *Science* **316**, 76–82 (2007).
45. Liu, X. et al. Optogenetic stimulation of a hippocampal engram activates fear memory recall. *Nature* **484**, 381–385 (2012).
46. Zhang, Y. et al. Dendritic channelopathies contribute to neocortical and sensory hyperexcitability in Fmr1−/y mice. *Nat. Neurosci.* **17**, 1701–1709 (2014).

Acknowledgements

We thank past and current members of the Frick and Bontempi laboratories for fruitful discussions and comments that contributed to the progress of this project. We thank Marie DeGrave, Elodie Cougouilles for assistance with behavioral experiments and Francesca Bettoni for assistance with neuronal reconstructions. We thank Dr. Ourania Semelidou and Dr. Marie Oulé for feedback on the manuscript. We thank Dr. Aline Desmedt for providing access to her behavioral equipment. We thank the genotyping and animal housing facilities of INSERM U1215 Neurocentre Magendie for ensuring the welfare of the laboratory animals. We would like to acknowledge the Bordeaux Imaging Center, a service unit of CNRS-INSERM and Bordeaux University and member of the national infrastructure France BioImaging supported by the French National Research Agency (ANR-10-INBS-04), and Dr. Monica Fernandez Monreal and Sebastien Marais for their technical assistance with microscopy and image analysis. We thank Dr. Susumu Tonegawa (MIT) for kindly providing the plasmids for activity-dependent neuronal labeling. This work was funded by grants from the Agence Nationale pour la Recherche (ANR-15-CE37-0013-01 and 02, project CORTMEM to AF and BB; ANR-23-CE37-0013-02, project Thalagram to BB), Région Nouvelle-Aquitaine (AAPR2024I-2023-32085510 to BB), the CNRS, INSERM, and the University of Bordeaux. BB also acknowledges support from the IHU 'Precision & Global Vascular Brain Health Institute–VBHI' funded by the France 2030 initiative (ANR-23-IAHU-0001). BB and ON also received financial support from the French government in the framework of the University of Bordeaux's IdEx "Investments for the Future" program (GPR BRAIN_2030). SH was supported by a post-doctoral allocation from the Région Nouvelle-Aquitaine (AAPR2024A-2023-32085810). LZ was supported by China Scholarship Council and MGC by University of the Basque Country - PIFBUR/20.

Author contributions

Conceptualization: S.H., M.G., B.B., and A.F. Experiments: S.H., L.Z., M.G., M.G.C., P.A.M., R.D.S., K.L.C., and O.N. Analysis: S.H., L.Z., M.G.C., and Y.L.F. Funding acquisition: L.Z., M.G.C., B.B., and A.F. Project administration: B.B. and A.F. Writing – original draft: S.H., L.Z., M.G., B.B., and A.F. Writing – review & editing: S.H., L.Z., M.G., Y.L.F., O.N., B.B., and A.F.

Competing interests

The authors declare no competing interests.

Additional information

Supplementary information The online version contains supplementary material available at https://doi.org/10.1038/s41467-025-66975-3.

Correspondence and requests for materials should be addressed to Bruno Bontempi or Andreas Frick.

Peer review information *Nature Communications* thanks Yuji Ikegaya, and the other, anonymous, reviewer(s) for their contribution to the peer review of this work. A peer review file is available.